Plasma Chemistry and Plasma Processing (2026) 46:95
https://doi.org/10.1007/s11090-026-10703-2

ORIGINAL PAPER

Performance and Reaction Mechanisms of an Indoor Air Decontamination System Combining Non-thermal Plasma and Photocatalyst for VOC Removal

Alex Destrieux[1] · **Zdenko Machala**[1]

Received: 26 March 2026 / Accepted: 27 July 2026

Abstract
An indoor air decontamination system combining a dielectric barrier discharge (DBD), UV-C lamps, and a TiO_2 photocatalyst, is investigated for the simultaneous removal of two volatile organic compounds (VOCs) — formaldehyde and methanol — at a high flow rate of 300 $L \cdot min^{-1}$. The contributions of each component are evaluated independently and in combination, showing a strong synergistic effect between DBD and UV-C, particularly for formaldehyde removal, reaching up to 50% efficiency in a single pass at 60% relative humidity — even in the absence of TiO_2. The photocatalyst is found to significantly improve the removal efficiency of methanol, which is detrimental to formaldehyde removal efficiency. The effect of specific input energy (SIE) is examined, showing that combining DBD with UV-C at equivalent SIE outperforms the discharge alone by a factor of two or more. The underlying degradation mechanisms are discussed in detail, identifying oxygen atoms, OH radicals, and several indirect OH reservoirs as key contributors. A notable observation is the release of NO_2 upon UV-C ignition following the discharge operation, attributed to the photodesorption of surface nitrates accumulated on TiO_2 during plasma exposure, which temporarily scavenges OH radicals and reduces removal efficiency.

Keywords Indoor air decontamination · Dielectric barrier discharge · Photocatalysis · TiO_2, VOC removal

Introduction

Indoor air pollution (IAP) has become a major public health risk, as people spend more than 80% of their time in indoor environments. The World Health Organization estimated the number of deaths caused by household air pollution to be around 2.9 million deaths in 2021 [1]. The three main types of indoor air pollutants are volatile organic compounds (VOCs),

✉ Zdenko Machala
machala@fmph.uniba.sk

[1] Faculty of Mathematics, Physics, and Informatics, Comenius University Bratislava, Bratislava, Slovakia

Published online: 04 August 2026

biological contaminants, and particulate matter. VOCs, the most common type of pollutants, originate from numerous sources including building materials, furniture, cleaning products, paints, solvents, and human activities. Exposure to VOCs such as formaldehyde (CH_2O), acetone, benzene or toluene can lead to eyes, nose and throat irritation, headaches, nausea, can cause damage to liver, kidney and central nervous system, and even cause cancers [2]. The development of efficient technologies for IAP control hence remains a major challenge.

Various technologies already exist for indoor air purification. The best-known one is the so-called high-efficiency particulate air (HEPA) filter. While HEPA filters achieve efficiencies higher than 99.97% [3] against particulate matter, they are usually inefficient against VOCs pollution. Other methods can be used, such as ionizers, electronic precipitation, adsorption by active carbon, or catalytic oxidation. However, while each of these techniques presents its advantages, several drawbacks can also limit their use. Especially, the frequent replacement of some parts (filters), the costs associated with maintenance, or the fact that they are nondestructive and hence generate secondary undesirable pollution, can be cited. For these reasons, developing technologies which could completely mineralize the VOCs to H_2O and CO_2 have intensively been studied over the past few years.

Among these advanced oxidation processes, the two main ones that can be distinguished are non-thermal plasma (NTP) and photocatalytic oxidation (PCO). The latter employs semiconductor materials, which under specific light illumination, generate electron-hole pairs. In turn, those can further react with ambient moist air to produce reactive oxygen species (ROS) such as hydroxyl radicals (OH) and superoxide radicals (O_2^-). These ROS can oxidize the VOCs adsorbed on the photocatalyst surface, converting them to H_2O, CO_2, or intermediate byproducts. The most typically used photocatalyst is titanium dioxide (TiO_2), due to its low cost, non-toxicity and good stability. Several recent reviews have summarized the advances on TiO_2 research, highlighting that TiO_2 can effectively fully mineralize VOCs. Several ways to improve the typical limiting factors in terms of VOCs conversion are also presented, such as doping or surface engineering approaches [4, 5]. Experimental studies have also shown high efficiencies of VOCs removal with TiO_2. For instance, Hanif et al. [6] achieved formaldehyde degradation around 70% within one hour of UV irradiation using TiO_2 incorporated in polypropylene membranes. In another study on CH_2O removal from Wang et al. [7], Ag/ZSM-5/g-C_3N_4/TiO_2 composite photocatalysts reached 93% efficiency, mostly attributed to increased adsorption capacity and improved charge separation within the heterojunction structure. High performance of modified TiO_2/sepiolite composites have also been reported by Song et al. [8]. Within 90 min of UV irradiation, CH_2O was degraded with about 87.6% efficiency. Such material can be interesting for ecofriendly substitutions as it is a natural material.

Concerning the second advanced oxidation technique, NTP has been extensively studied for this purpose. Contrarily to thermal plasmas, NTP allows the generation of high energy electrons while maintaining the gas around ambient temperature. Those high energy electrons can then generate oxidative species, such as ROS, oxygen atoms (O) or ozone (O_3), which can oxidize VOCs. Early studies showed that NTP alone could efficiently decompose VOCs from air steams [9]. Kim et al. [10]. provided a comprehensive review of pollution control with NTP, describing the chemistry of the VOCs degradation, the importance of ROS, as well as the different discharge configurations that could be used. Concerning more recent experimental works, several papers focused on the VOC abatement using dielectric barrier discharges (DBD). Asilevi et al. [11]. reached a degradation of CH_2O of 99% using

an atmospheric pressure DBD operating in dry air. Such results were obtained with low initial concentrations of CH_2O (< 1 ppm). Similarly, Mustafa et al. [12]. achieved a complete removal of several VOCs (benzene, toluene, trichloroethylene, and tetrachloroethylene) using NTP alone in a double DBD configuration. Those results were obtained with 100 ppm as initial concentration, low gas flow rates of 1 $L.min^{-1}$ and around 50 W of discharge power. Other studies have shown the efficiency of NTP at removing aromatic VOCs. Saleem et al. [13]. employed a coaxial DBD reactor to remove toluene from CH_4 (application to biogas). While they obtained efficiencies up to 86%, their paper also emphasizes the influence of the power and flow rate on the performance of the system. Other types of VOCs, such as oxygenated ones (methanol for example), can be removed with very high efficiencies up to 97% [14]. While both NTP and photocatalysis have shown very good potential for the VOCs abatement, they still present some limits. For the photocatalyst, most of the examples mentioned advanced modified TiO_2 or composite materials, which may not be as easy to obtain as pristine TiO_2. For NTP, one of the big challenges is power consumption which is typically high. Additionally, incomplete mineralization is often observed, and low air flow rates are used for lab-scale studies, which is far from real environmental applications.

For these reasons, researchers have developed hybrid systems combining NTP + PCO. This combination employs the two advantages of both technologies to decompose VOCs even more efficiently. Especially, new reactions pathways can appear when the NTP generated byproducts interact with the catalyst's surface. Recent reviews highlighted the synergetic effect between these two technologies, especially the plasma induced catalyst activation, enhanced ROS generation, as well as the decomposition of the plasma-generated byproducts by the photocatalyst [15, 16]. The potential of these combined technologies has been proven experimentally. Li et al. [17]. used a coaxial DBD reactor filled with different photocatalysts (all TiO_2 based) to remove toluene from air. The best results obtained were with Ag-TiO_2/γ-Al_2O_3 catalyst, reaching complete toluene removal with around 80% CO_2 selectivity. Jangra et al. [18]. developed a surface DBD with a TiO_2 modified sheet as a ground electrode. In this case, no UV light is required and the photocatalyst is activated by the discharge. They removed toluene and benzene with 99.7% and 74.8% efficiency, respectively. More recently, Vazquez et al. [19] attempted to scale up a DBD + PCO reactor. They employed a DBD and 4 UV lamps, enclosed in a TiO_2 textile cylinder to treat high flow rates of polluted air (250 $L.min^{-1}$). The best efficiency reached there was 40% for CH_2O removal.

While the performances of those combined systems are very promising, Vazquez et al. [19] shows one of the main limits to real applications, which is the scaling up of NTP + PCO technologies to reach *high removal efficiencies at high flow rates*. The current study follows this paper. As they assessed preliminary results for VOCs removal and bio-decontamination, this paper focuses deeper on formaldehyde and methanol removal from ambient air, in a single-pass configuration at a *high flow rate of 300 L.min*$^{-1}$. The emphasis is put on both the *performance* of the system, as well as the *reaction mechanisms* involved in the degradation. The first part is dedicated to the evaluation of the effect of the different components of the system. The removal efficiency, the concentration of pollutants and byproducts are discussed. The effect of the specific input energy (SIE) is also investigated. The second part intends to discuss the possible reaction pathways, and focuses on CO and NO_2 byproducts.

Materials and Methods

Indoor Air Decontamination System

The indoor air cleaning system, shown in Fig. 1 has already been presented in our previous study [19]. The different components are enclosed in an airtight chamber separated into two compartments. The first one contains a bubbling system to inject the vapors of the test pollutants and a fan sucking the latter, mixed with the ambient air, to the decontamination chamber. To produce the VOCs in the gas phase, 2 $L.min^{-1}$ of air flow was bubbled through a 36% solution of formaldehyde (CentralChem), stabilized with methanol (11%). Two pollutants are hence inserted simultaneously during the experiments. The total air flow was fixed for all experiments at 300 $L.min^{-1}$. Due to the high flow rates, the system is using the ambient air, which is subject to relative humidity (RH) variations, usually ranging from 20% to 60%.

The second compartment is the decontamination chamber. It is the main core of the system and consists of the DBD and the 4 UV-C lamps (Philips TUV PL-L 35 W/4P HO 1CT/25, electrical power input 35 W, UV radiated power 9.1 W, 254 nm), both enclosed in the cylindrical cage wrapped with a textile with TiO_2 layer (20 cm diameter, 30 cm length, surface 1884 cm^2). The anatase TiO_2 photocatalyst (Ahlstrom, Finland) is deposited on a non-woven cellulose/polyester matrix, with a density around 20 g/m^2. The TiO_2 nanoparticles have a diameter of ~10 nm. The thickness of the layer (TiO_2 + textile support) is around 125 µm. The original commercial product contains an active carbon layer, which is completely removed prior to the experiments to ensure that no adsorption/desorption occurs. This was tested by running VOCs with and without the TiO_2 layer, and no difference in concentration was observed. Similarly, when the VOC flow is turned off, CH_3OH and CH_2O are not detected in the FTIR spectra, indicating that they are neither accumulated on nor desorbed from the TiO_2 layer.

The 4 UV-C lamps are positioned in a "cross" way (see Fig. 1, right) to ensure a homogeneous illumination of the TiO_2. Note that the ignition of the UV-C lamps in the system lead to a slight temperature increase of the TiO_2. The latter was measured on the outer surface of the TiO_2 layer using an infrared thermometer. For 2 UV-C lamps, the temperature raised by 6 °C, and for 4 UV-C lamps by 11 °C.

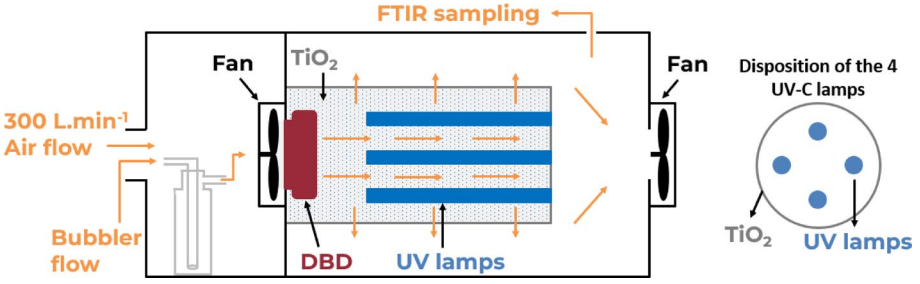

Fig. 1 Schematic of the indoor air cleaning system. The left compartment contains the bubbling system with the liquid pollutant. The right compartment contains the decontamination part, with the DBD, the UV-C lamps and the cage wrapped with the textile containing TiO_2. The disposition of the 4 UV-C lamps inside the cage is shown on the right side

The DBD module is made of 17 alumina ceramic tubes (3 mm diameter, wall thickness 0.75 mm), each tube being alternately connected to the ground and high voltage of the power supply. The gap between each two adjacent ceramic tubes is 1.25 mm. The power supply used is PVM500 (Information Unlimited, USA). As it is based on resonance, the DBD is always powered by a 36 kHz sine waveform. As the power supply regulates the current, the power can be tuned up to 150 W, with a typical applied voltage lying between 13.5 kV_{pp} to 15 kV_{pp}. All electrical measurements are retrieved during the experiments using a North Star PVM12 high voltage probe, a Pearson 2877 current probe, and the charge is determined by measuring the voltage across a 40.37 nF capacitor with a Tektronix TPP0201 passive probe. The power is determined using the classical Lissajous method [20]. The DBD generated operates in the typical filamentary mode at atmospheric pressure.

The geometry has been designed to have all the treated air passing through the discharge and the UV activated TiO_2 layer. Once treated, a peristatic pump sucks 2 $L.min^{-1}$ of air to be analyzed by Fourier-transform infrared spectroscopy (FTIR), and the remaining air is evacuated from the chamber. It should be noted that all experimental results obtained correspond to a single-pass of the polluted air through the system, with no air recycling.

FTIR Analysis

FTIR (Shimadzu IRSpirit-T) is the main analytical tool used to evaluate the efficiency of the indoor air decontamination chamber. As the concentrations of input VOCs and consequent byproducts are low, around 10 ppm, a 5-m long path cell is used (Cyclone C5 from Specac, 2 L cell). FTIR spectra were acquired with a 0.9 cm^{-1} resolution, and 40 scans were accumulated, which took 210 s per spectrum. The background for all experiments was taken with the 300 $L.min^{-1}$ of air flowing through the reactor, without pollutant. A typical spectrum obtained after passing the VOCs containing air through the decontamination chamber is shown in Fig. 2.To extract the concentrations of different species, experimental data were manually fitted using the data from Hitran database. The signatures of the unfragmented formaldehyde and methanol appear between 2750 cm^{-1} and 3050 cm^{-1} (C-H stretch, individual signatures in the red box zoom). The region between 2750 cm^{-1} and 2830 cm^{-1} was used for CH_2O concentration determination, as higher wavenumbers overlap with CH_3OH. The region from 2020 cm^{-1} to 2260 cm^{-1} displays three compounds generated by the DBD, i.e., nitrous oxide (N_2O), carbon monoxide (CO) and ozone (O_3). Another plasma generated species, e.g. N_2O_5, was also monitored during experiments (1240 cm^{-1} and 1275 cm^{-1}). The main signal from formaldehyde (C = O band) can also be observed between 1670 cm^{-1} and 1825 cm^{-1}. However, due to the overlap with water vapor and N_2O_5, this band was not used for the concentration estimation. Finally, concentration of methanol was retrieved from the 2750 cm^{-1} – 3050 cm^{-1} region. Knowing the ozone concentration from the 2050 cm^{-1} – 2150 cm^{-1} band, it was possible to use it to obtain a good fit of the methanol by summing the two spectra. For the VOC removal, the removal efficiency is calculated as [21]:

$$\eta = \frac{[VOC_{in}] - [VOC_{out}]}{[VOC_{in}]} \quad (1)$$

With VOC_{in} and VOC_{out} the input and output VOCs concentrations, respectively.

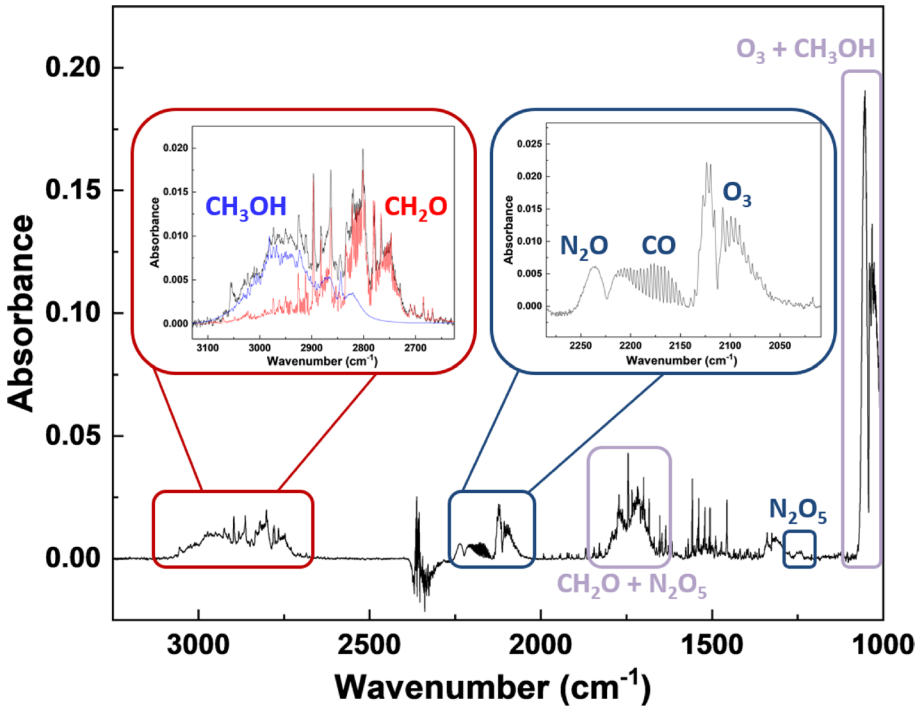

Fig. 2 Typical FTIR spectra obtained after passing the polluted air through both the DBD and the UV-activated TiO_2 layer, with a 0.9 cm^{-1} resolution and 40 scans

Results and Discussion

Effect of the Different Components of the System

To better evaluate the global operation of the system for VOCs removal, the starting point is to understand the effect of each component, i.e., the DBD, the UV-C lamps, their combination, as well as the effect of TiO_2. For each condition, the VOCs and the total air flow are set (300 $L.min^{-1}$) and run for ten minutes to reach a steady state condition, and 3 spectra are taken to get the input VOC concentration. The relative humidity (RH) was 50%. Then each component tested is ignited, and the spectrum acquisition started at least one minute later, the time for the gas to fill the long-pass cell. Five spectra are taken for each condition. For the conditions where the DBD is operating, its power was set to 120 W.

The results obtained for the removal efficiency of both formaldehyde and methanol are shown in Fig. 3. Note that no standard deviations are plot on the figure. The experiments were repeated several times and showed the same trends, However, due to variations of the relative humidity (not controlled in ambient air condition) as well as the input concentration of VOC, it is difficult to plot proper standard deviations that would be representative of all the experiments. Going to the results, first, the UV-C lamps alone have no effect on removing VOCs when no TiO_2 layer is present. When the TiO_2 layer is added to the system with UV-C on, the VOCs start to be removed, reaching 14% degradation for CH_2O and 10% for CH_3OH. The removal efficiency seems low, but it should be noted that this is a single-pass

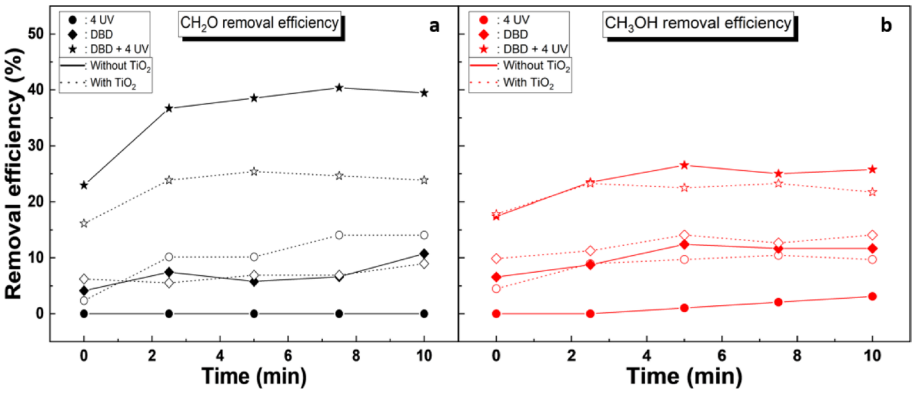

Fig. 3 Effect of the components of the system (DBD, UV-C lamps, both combined) on the removal efficiency of (**a**) formaldehyde and (**b**) methanol. Full lines represent the experiments without TiO_2 layer, and dotted lines with TiO_2 layer

system operating at high air flow rate. Then, when testing the efficiency of DBD alone, the results show that the TiO_2 layer does not play any role. The efficiency slightly varied, with lower values on the first points, which could be due to the delay in the gas renewal in the long path cell. Still, the maximum removal efficiency obtained is 14% for methanol and only 11% for formaldehyde. When combining the DBD and 4 UV-C lamps, better efficiency is achieved. In the case of methanol, it fluctuates between 22% and 26%, both with and without TiO_2, which corresponds approximately to the sum of the two components separated.

On the other hand, an interesting behavior can be observed for formaldehyde. When the TiO_2 layer is present, the same trend as methanol is observed, i.e., the achieved efficiency when combining DBD and UV is around 23% −24%, close to the sum of the two components alone. However, when the TiO_2 layer is removed, the measured efficiency is significantly higher, reaching 40%. This is especially noteworthy since the UV-C lamps alone have no effect when the TiO_2 layer is not present in the system. While the mechanisms behind this behavior are not yet clear, the experiments presented here show the synergetic effect between plasma and photocatalyst.

Species Concentrations and Main Byproducts

It was shown in the previous section that, even with a high air flow rate of 300 $L.min^{-1}$ and single-pass, relatively good VOC removal efficiency could be achieved, especially against formaldehyde (40%). This section intends to evaluate the concentrations of the different species again depending on which component of the system is operating, especially focusing on different byproducts.

To do so, the different components of the system were switched on successively. The DBD was ignited first, the power being set to 120 W. Then 2 and 4 UV-C lamps were added in combination with the discharge. Finally, the DBD was switched off to compare with the photocatalytic effect alone. This sequence was performed both with and without the TiO_2 layer. VOCs concentrations have been measured prior and after the operation of the different components. For each condition, three FTIR spectra were taken. Results are shown in Fig. 4 for two different relative humidities, 30% and 60%. The full lines represent the experiment

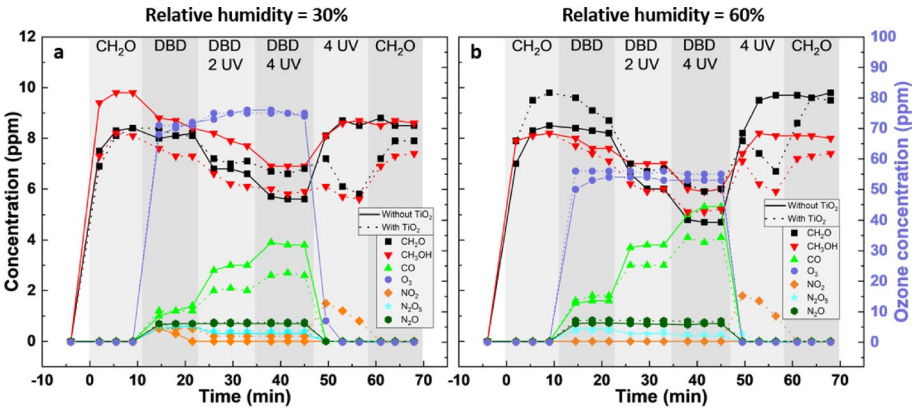

Fig. 4 Evolution of the concentration of the different species when the different components of the system are operating. Experimental conditions: air flow rate 300 L.min^{-1}, P_{DBD} = 120 W. The relative humidity was (**a**) RH = 30% and (b) RH = 60%

without the TiO_2 layer, and dotted lines with the TiO_2 added. Note that the methanol concentration is the same for both experiments, and initial and final concentrations are almost the same. However, a deviation is observed for formaldehyde, which initial value was slightly lower for the experiment without TiO_2, but increased and the final concentration matched the condition with TiO_2. This effect was accounted for by interpolating the formaldehyde concentration, considering a linear increase between the initial and final values, when calculating the efficiency (see Sect. 3.3).

When the discharge is first ignited, for both relative humidities, a slight drop of both CH_3OH and CH_2O concentrations is observed, either with or without TiO_2. Similarly, when 2 or 4 UV-C lamps are ignited, both concentrations decrease even more, this effect is accentuated by the number of lamps. Then, the discharge is switched off, and only the UV-C lamps remain operating. As it was seen before, without TiO_2 no destruction of the pollutants is observed so their concentration increases. But with TiO_2, both CH_3OH and CH_2O concentrations first rise after the discharge extinction and then start dropping again. This could indicate a change in the chemistry degradation of the pollutants. Note that, for the two relative humidities tested, the trends are the same. The main difference lies in the removal efficiency. At 30% RH, in the best case, the CH_2O concentration drops from 8.4 ppm to 5.6 ppm, giving an efficiency of 33%. Similarly, at 60% RH, the strongest decrease for CH_2O is from 8.5 ppm to 4.7 ppm, leading to an efficiency of 45%. Generally, for both pollutants, the amplitude of the decrease is the highest at higher relative humidity. Such an effect is already well known, as increased relative humidity favors the generation of OH radicals, oxidizing the VOCs [11].

Concerning the byproducts, the main ones detected are O_3, NO_2, N_2O, N_2O_5 and CO. All of them, except CO, are typical species generated by atmospheric pressure DBD in nitrogen/oxygen mixtures [22]. As can be seen on Fig. 4, O_3 and N_2O were constant over the discharge operating time and seem to be independent of the UV-C lamps. It is also interesting to notice the lower concentration of ozone with higher humidity. This is expected due to the increased generation of OH radicals, which partially reduce ozone [23]. N_2O_5 is also present all along with the discharge operation but shows a slight decay with the UV-C lamps igni-

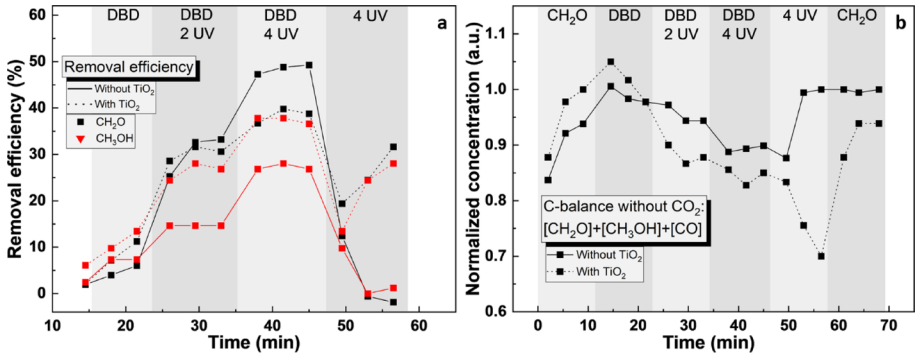

Fig. 5 (**a**) Removal efficiency of CH_2O and CH_3OH with and without TiO_2 layer obtained from experimental concentrations shown in Fig. 4. (**b**) Partial carbon balance (sum of CO, CH_2O and CH_3OH concentrations) depending on which component of the system is operating

Table 1 Summary of the removal efficiency obtained in Fig. 5a. Each value in the table is the mean value of the three *experimental points for each condition*

	CONDITION							
	DBD		DBD+2 UV		DBD+4 UV		4 UV	
	TiO_2	No TiO_2	TiO_2	No TiO_2	TiO_2	No TiO_2	TiO_2	No TiO_2
η_{CH_2O} (%)	6.8	4.0	30.3	30.3	38.4	48.4	25.2	4.1
η_{CH_3OH} (%)	9.7	5.7	26.4	14.6	37.4	27.7	21.9	3.7

tion. This must be taken carefully as the concentrations measured here are very low (0.2–0.5 ppm), so this slight drop could also be due to the measurement error or the presence of water vapor, making the quantification complicated. The last byproduct which is very likely produced is CO_2. Since the VOC concentrations were only 9–12 ppm, the possible generated CO_2 concentrations were also likely be only a few ppm, but it is impossible to measure such low CO_2 concentration as it is negligible compared to the CO_2 present in the ambient room air used during the experiments (typical indoor values vary within 500–1000 ppm).

Another interesting behavior here is the NO_2 formation. The latter is not observed during the discharge operation but rather appears when the DBD is switched off and the UV-C lamps remain active, only in the case where TiO_2 is present. This case will be discussed later in Sect. 4.

Finally, the last byproduct is carbon monoxide. Its concentration follows the opposite trend than that of CH_2O and CH_3OH, indicating it is a byproduct of the pollutant fragmentation. It reaches a maximum of 5.3 ppm in the case with DBD and UV-C lamps without TiO_2, simultaneously corresponding to the minimum pollutant concentration.

Removal Efficiency and Partial Carbon Balance

Using the evolution of the concentrations obtained in Fig. 4b, it is possible to calculate the removal efficiency of the system for the two contaminants. Results are shown in Fig. 5a. The removal efficiency obtained for each condition is also reported in Table 1. The values provided there are the mean values of the three points of each experimental condition. As expected, the removal efficiency is again low for the DBD alone, with less than 10% for

all the cases. With 2 UV-C lamps added, the efficiency rises to around 30%, except for the CH_3OH without TiO_2, which remains around 15%. With then 4 UV-C lamps, efficiency reaches its maximum for all the conditions. The highest efficiency is 48.4% for CH_2O without TiO_2. However, this also corresponds to the lowest CH_3OH removal efficiency with 27.7% for the DBD+4 UV-C lamps condition, while with the TiO_2 layer, both pollutants are removed with around 38% efficiency.

Finally, the DBD is switched off, and 4 UV-C lamps remain ignited. Again, without TiO_2, efficiency drops close to 0% for the two pollutants. With TiO_2, the efficiency first drops for CH_3OH and CH_2O to around 20%, before rising again to close to 30% (mean efficiency of 21.9% and 25.2%, respectively). Two main points should be noted regarding those results. The first one is the efficiency achieved in a single pass at high flow rates which is quite high for the DBD+4 UV-C lamps condition. But here, the absence of TiO_2 seems to enhance the conversion of formaldehyde over the one of methanol, while when TiO_2 is present, both conversion levels are similar. The second point concerns the photocatalytic effect. From the single components presented in Sect. 3.1, the best efficiency reached was around 10% for both pollutants simultaneously. However, in Fig. 5a, after dropping, the efficiency increases to 30% for CH_3OH and CH_2O. The main difference is that here, the discharge was operating beforehand. Efficiency could be enhanced by some mechanisms or species generated by the discharge and accumulated on the TiO_2. This possibility will be discussed in more detail in the section dedicated to the reaction mechanisms (Sect. 4).

As carbon monoxide is the only carbon containing byproduct, it is possible to sum it with the pollutants' concentration to obtain a partial carbon balance. The latter is only partial, as the precise CO_2 concentration could not be measured in this configuration due to its much higher background concentration in air. The results are presented in Fig. 5b. The two plots here are normalized: with TiO_2 the initial and final concentrations being almost the same, the initial value was taken as a reference. However, without TiO_2, as mentioned previously, initial value was lower than the final value. The latter was chosen for normalization. With the DBD alone ignited, the normalized concentration remains around one or even slightly higher, with and without TiO_2. This more likely means that CO is the main byproduct from the pollutants' decomposition. With 2 UV-C lamps added to the DBD, the normalized concentration starts to reduce. Without TiO_2 it drops 0.94, and around 0.86 with TiO_2. As the value departs from the nominal value of 1, it indicates that byproducts other than CO are formed but not detected. As can be expected, going with then 4 UV-C lamps along with the DBD, the normalized concentration drops even more, reaching 0.89 without photocatalyst, and 0.84 with it. Concerning the pure photocatalytic effect, i.e., without DBD, without TiO_2 the normalized concentration goes back to its nominal value, as no pollutant conversion was observed. But with TiO_2, the value drastically diminishes, reaching a minimum of 0.7. As no CO was detected in this case, the main byproduct is different, most likely CO_2.

This section showed that good efficiencies could be obtained, even in a single pass configuration with high air flow rates. While without TiO_2 the efficiency was better for CH_2O than CH_3OH, adding then the TiO_2 layer enhanced the CH_3OH degradation but slightly reduced that of CH_2O. The partial carbon balance suggested an incomplete mineralization of the pollutant, as CO is the main byproduct. However, especially in the case of purely photocatalytic effect, no CO is detected, which could hence promote the formation of CO_2. The next section focuses on the effect of the specific input energy on the degradation of the pollutants.

Effect of the Specific Input Energy

The specific input energy (SIE) is an important parameter for pollutant removal. Higher SIE, especially due to the power increase of the discharge, tends to generate higher electron densities and energy, as well as increased concentrations of reactive species. The SIE is defined as:

$$SIE\,(J.L^{-1}) = \frac{P\,(W)}{Q(L.s^{-1})} \tag{2}$$

With P the power injected (in this case $P = P_{DBD} + P_{UV}$) and Q the flow rate ($300\ L.min^{-1}$). Experiments were carried out again with and without the TiO_2 layer, for three discharge power: 50 W, 130 W and 165 W. For each power, the removal efficiency was measured with and without the UV lamps (4 lamps, $P_{UV} = 36.4\,W$) as well. The relative humidity was 20%. For each condition, three measurements were performed, and the results in Fig. 6a and b show the mean values and the corresponding standard deviations (SD).

Focusing first on the removal efficiency when the discharge was operating alone, the results are similar whether TiO_2 is present or not. In both cases, taking the SD into account, the removal efficiency for CH_2O was the same. For CH_3OH, the removal efficiency values were slightly higher with the TiO_2 layer. This could be due to enhanced interactions with the radicals at the photocatalyst surface even if the latter is not activated. But generally, it is expected that without activation of the TiO_2 and the DBD operating alone, the same trends are observed.

With the UV-C lamps added, interesting results can be observed. In both cases, with and without TiO_2 layer, the removal efficiency increased with the higher SIE, whatever the pollutant. Without TiO_2 (Fig. 6a), the system is more efficient at removing CH_2O rather than CH_3OH (39.6% and 26.8% at 40 $J.L^{-1}$, respectively). As can also be seen in this case, increasing the SIE from 34 $J.L^{-1}$ to 40 $J.L^{-1}$ almost doesn't change the efficiency of the process. With TiO_2 (Fig. 6b), CH_3OH is preferentially removed with 41.3% efficiency, against 23.5% for CH_2O at the highest SIE. There, compared to the condition without TiO_2, the rise in SIE from 34 $J.L^{-1}$ to 40 $J.L^{-1}$ still leads to an improved efficiency, going from 32.6% to 41.3%, respectively. In contrast, the removal efficiency of CH_2O is barely affected, espe-

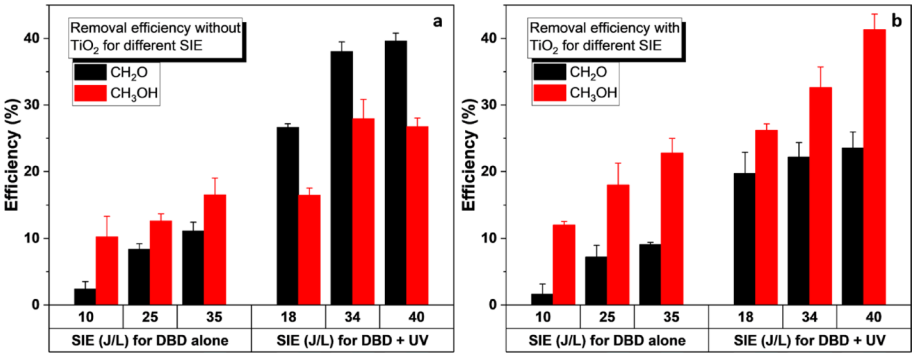

Fig. 6 Removal efficiency as a function of the specific input energy for the DBD and DBD + UV measured (**a**) without TiO_2 and (**b**) with TiO_2

cially considering the SD. Another very interesting behavior concerns the comparison of the conditions with almost the same SIE, i.e., the one with the DBD alone (35 $J.L^{-1}$) and the one with DBD+UV (34 $J.L^{-1}$). In that case, the discharge power is 165 W for the discharge alone, and 130 W for the discharge with the UV-C lamps (here $P_{DBD} = 130\,W$ and $P_{UV} = 36.4\,W$). Without TiO_2, when adding the UV-C lamps (and hence decreasing P_{DBD} to keep the SIE constant), the removal efficiency for CH_2O rises from 11.1% to 38.0%, and from 16.5% to 28% for CH_3OH. With TiO_2 the effect is less pronounced but still visible, with an increase of 9% to 22.1% for CH_2O and 22.8% to 32.6% for CH_3OH. Such behavior shows again the improved efficiency brought by the synergy between the discharge and the UV radiation, even when TiO_2 is not present.

Using the efficiencies values from Fig. 6, it is possible to estimate the energy yield in g/kWh for the VOC removal process. The energy yield is defined as:

$$Energy\ yield\ (g/kWh) = \frac{Mass\ removed\ per\ hour\ (g/h)}{Power\ (kW)} \tag{3}$$

More details about the calculations can be found elsewhere [19]. The energy yield is calculated for the best efficiencies with and without the TiO_2 photocatalyst, and for the discharge alone or in combination with the 4 UV-C lamps. The values are calculated for two different powers: the total electrical input power, which considers the electrical input power of the UV-C lamps and the power measured at the socket of the power supply, or the gas input power, which considers only the radiated UV power and the discharge power. The values are presented in Table 2.

Note that the energy yield given is summing up the amount of both CH_2O and CH_3OH removed simultaneously during the process. As one can expect, the energy yield is lower when the total electrical input power is taken for the calculation. Even in this case, the values are slightly underestimated as the power of the fans is not considered. The best energy yield taking the total power is 0.44 g/kWh. Taking the power delivered to the gas, the best energy yield only increases to 0.77 g/kWh for the DBD + 4 UV-C lamps, both with and without TiO_2. Even with the good removal efficiencies at low SIE due to the high flow rates, the energy yield is still limited. To compare with the literature, Asilevi et al. [24]. used a double gap DBD to remove CH_2O from a polluted air stream. They estimated an energy yield for their system of 1.25 g/kWh. However, in their case, the SIE was 2500 $J.L^{-1}$, which is two orders of magnitude higher than in the current work. Similarly, Dhakal et al. [25]. employed a multi-electrode cylindrical DBD system for formaldehyde removal. Their system reached an energy yield of 2.53 g/kWh for a SIE of 450 $J.L^{-1}$.

Table 2 Energy yield of the process values calculated from the best efficiencies obtained in Fig. 6 for formaldehyde and methanol. The initial concentrations are in the range 9–12 ppm

Condition		Efficiency (%)		Energy yield (g/kWh)	
		CH_2O	CH_3OH	Total power	Gas power
Without TiO_2	DBD	11.1	16.5	0.19	0.30
	DBD+4 UV-C	39.6	26.8	0.44	0.72
With TiO_2	DBD	9.1	22.8	0.21	0.34
	DBD+4 UV-C	23.5	41.3	0.44	0.71

This section showed interesting results on the effect of SIE on the pollutant removal efficiency. While the results were similar when discharge operates alone, with and without TiO_2, different trends were observed when the UV-C lamps were added. In that case, CH_2O seems to be preferentially removed without TiO_2, while CH_3OH is more efficiently removed with TiO_2. It was also seen that, for the same SIE, combining DBD and UV-C lamps led to a drastically improved efficiency by a factor 2 or more. Finally, the energy yield was calculated. While the values are below 1 g/kWh and are lower than the values that can be found in the literature, the results are still promising, as the SIE is one to two orders of magnitude lower compared to other studies. Note that, compared to many works in the literature, achieving comparably high energy yields is impossible, since the initial concentrations of pollutants are very low (~10 ppm) in this study. The next section intends to discuss different mechanisms involved in the degradation of the pollutants.

Reaction Mechanisms

In the previous sections, several trends have been observed. Especially, depending on the operating system components, different efficiencies or byproducts concentrations were highlighted. This section intends to unravel the different mechanisms involved in the degradation of formaldehyde and methanol, while assessing how the discharge, the UV-C lamps, and the TiO_2 can modify or add new degradation pathways.

Plasma Degradation Mechanisms

The main reactive species generated by the discharge are electrons, as well as atomic oxygen (O) and hydroxyl radicals (OH). These two are generated via:

$$e^- + O_2 \rightarrow 2O + e^- \quad \text{(R1)}$$

$$e^- + H_2O \rightarrow OH + H + e^- \quad \text{(R2)}$$

Electrons, O and OH can then initiate the first reactions with CH_3OH [26–28] and CH_2O [25, 29]:

- Electron impact dissociation.

$$CH_2O + e^- \rightarrow HCO + H + e^- \quad \text{(R3)}$$

$$CH_3OH + e^- \rightarrow CH_2OH + H + e^- \quad \text{(R4)}$$

$$CH_3OH + e^- \rightarrow CH_3O + H + e^- \quad \text{(R5)}$$

- Oxidation by Atomic Oxygen.

$$CH_2O + O \rightarrow HCO + OH \quad \text{(R6)}$$

$$CH_3OH + O \rightarrow CH_2OH + OH \quad \text{(R7)}$$

- Hydroxyl radical oxidation.

$$CH_2O + OH \rightarrow HCO + H_2O \quad \text{(R8)}$$

$$CH_3OH + OH \rightarrow CH_2OH + H_2O \quad \text{(R9)}$$

Reactions R3 – R9 are the main mechanisms involved in the first step degradation of the pollutants. The direct electron impact dissociation of VOCs might not be the main degradation pathway. Most of the electron energy is dissipated by much more probably collisions with the main components of the gas, i.e., O_2 (R1), N_2 (dissociation or vibrational excitation) and to some extent H_2O vapor (R2). One interesting point to notice here is the presence of CH_2O as a byproduct of CH_3OH degradation (R8). This is important, since it can limit the efficiency of the system, as CH_2O is partially reformed during the conversion. Another important point is the formation of OH through reactions R6 and R7. While the pollutants react with oxygen atoms, the OH radicals formed can again react through reactions R8 and R9 to further improve the removal efficiency of both pollutants.

From the above reactions, three new byproducts are formed, which can further react:

$$CH_2OH + O_2 \rightarrow CH_2O + HO_2 \quad \text{(R10)}$$

$$HCO + O_2 \rightarrow CO + HO_2 \quad \text{(R11)}$$

$$CH_3O + O_2 \rightarrow CH_2O + HO_2 \quad \text{(R12)}$$

At this stage, it appears that different byproducts originating from methanol all form formaldehyde. In terms of efficiency this explains why, with the discharge alone, the methanol removal efficiency was higher than the formaldehyde one (see Fig. 6). Concerning the byproducts' degradation, two other points can be highlighted. First, the main degradation pathway of formaldehyde is through HCO radicals, which leads to the formation of CO. This is in good agreement with the experimentally observed CO formation, especially in the DBD operating alone, where CO_2 does not seem to be formed (see the partial carbon balance in Fig. 5b). The partial mineralization of CH_2O in low temperature plasma has already been studied, especially by Storch et al. [30]. Note that HCO radicals can also recombine together to reform CH_2O or react with OH to form formic acid. However, even if the rate constant of these two reactions has similar order of magnitude than reaction with O_2, the densities of HCO and OH radicals are low in comparison to O_2 molecules, thus the production rate of these two reactions is negligible. Second, in reactions R10 – R12, the second byproduct is always HO_2 radical. The latter can also induce beneficial reactions in the system [30–32]:

$$HO_2 + NO \rightarrow OH + NO_2 \quad \text{(R13)}$$

$$HO_2 + O \rightarrow OH + O_2 \quad \text{(R14)}$$

$$CH_3OH + HO_2 \rightarrow CH_2OH + H_2O_2 \quad \text{(R15)}$$

$$HO_2 + HO_2 \rightarrow H_2O_2 + O_2 \quad \text{(R16)}$$

$$HO_2 + OH \rightarrow O_2 + H_2O \quad \text{(R17)}$$

As can be seen, HO_2 can also be directly involved in the oxidation of methanol, forming hydroxymethyl radical and hydrogen peroxide (H_2O_2). The latter can react with O atoms to form OH radicals as well [33]:

$$H_2O_2 + O \rightarrow OH + HO_2 \quad \text{(R18)}$$

R18 is interesting, since it produces both OH radicals that can contribute to the pollutant degradation but also regenerates HO_2, which can again produce OH radicals through reactions R13 and R14. However, the rate constant of R18 is low, so it should not be a major contribution to the OH and HO_2 production. HO_2 can also recombine with itself (R16), producing H_2O_2, and undergo the pathway through reaction R18. Finally, HO_2 can also react

with OH radicals, terminating the reaction chain. Globally, while HO_2 is not the major direct pollutant oxidizing species in the system, it can still significantly contribute to the sustaining of the OH reservoir, improving the removal efficiency.

Effect of UV Radiation

The previously discussed mechanisms concerned the case when the discharge is operating alone. When adding UV-C lamps, even without photocatalyst, the removal was seen to improve (Fig. 3), especially for formaldehyde. One of the important species that has not been focused on is ozone. As it was measured during experiments (Fig. 4a and b), ozone concentration can reach several dozens of ppm. When oxygen atoms are generated in the discharge (R1), they can react with O_2 and a third body to form ozone [34]:

$$O_2 + O + M \rightarrow O_3 + M \tag{R19}$$

In the case of the discharge operating alone, reactions between ozone and CH_2O or CH_3OH exist, but their rate constants are very low. When adding the UV-C lamps with maximum radiation at 254 nm, in combination with the discharge, a new mechanism occurs, which is the photolysis of ozone [35]:

$$O_3 + hv \rightarrow O(^1D) + O_2 \tag{R20}$$

The generated $O(^1D)$ can react with water molecules to form OH radicals [36]:

$$O(^1D) + H_2O \rightarrow 2OH \tag{R21}$$

This is again a new source of production of OH radicals that can further enhance the degradation of methanol and formaldehyde. In the experiments performed, the decrease of ozone concentration is not so clear when the UV-C lamps are ignited. However, even a small fraction of the ozone converted to generated $O(^1D)$ and OH could already affect the removal efficiency. Especially, Vazquez et al. [19]. using the same experimental setup observed an ozone decrease when UV-C lamps were added, but at much lower concentrations (2 ppm of ozone). Additionally, the absorption cross section of ozone reaches its maximum at 254 nm, which is the exact emitting wavelength of the UV-C lamps. Such an effect can also contribute to the higher efficiency of the system at higher humidity (30% vs. 60%, Fig. 4), since more H_2O in the system can lead to more OH generation through reaction R21.

Another species mentioned previously can be photolyzed, which is hydrogen peroxide [37]:

$$H_2O_2 + hv \rightarrow 2OH \tag{R22}$$

In the same way that ozone in reaction R20, H_2O_2 is efficiently decomposed at 254 nm. Such reaction again enhances the generation of OH radicals. Experimentally, it was observed that combining the discharge with UV-C lamps, the removal efficiency improved for CH_3OH (up to 25%), and even more importantly for CH_2O (up to 40%). We saw that both VOCs react with OH radicals and O atoms (R6-R9). Concerning the rate constants, reaction of CH_2O (R6) with O atoms is approximately 2.5 times faster than CH_3OH (R7) with O, and CH_2O with OH radicals (R8) 10 times higher than CH_3OH with OH (R9). This means that, in the case of discharge alone, even if CH_2O reacts faster, the efficiency is balanced and limited by the reformation of CH_2O via CH_3OH degradation. But when the UV-C lamps are added, the extra OH generation might be much more beneficial to the destruction of CH_2O rather than that of CH_3OH, explaining the important increase for CH_2O observed in Fig. 3.

Photocatalytic Effect

As seen in Fig. 6, when the discharge operates alone, the presence or absence of TiO_2 did not change the removal efficiencies for formaldehyde and methanol. However, combined with UV-C lamps, clear differences were observed in removal efficiencies. This section is hence discussing the mechanisms concerning photoactivated TiO_2. The generation of electron-hole pairs on the TiO_2 surface occurs via [38]:

These electron-hole pairs generated on the photocatalyst can react with water or oxygen adsorbed on the surface to form reactive species:

$$TiO_2 + hv \rightarrow\ e^- + h^+ \tag{R23}$$

$$H_2O_{ads} + h^+ \rightarrow\ OH_{ads} + H^+ \tag{R24}$$

Through reactions R24 and R25, hydroxyl and superoxide radicals are formed, which are the main surface oxidative species. The first step is then the adsorption of VOCs on the TiO_2 surface [39, 40]:

$$O_{2,ads} + e^- \rightarrow\ O^-_{2,ads} \tag{R25}$$

$$CH_3OH + TiO_2^* \rightarrow\ CH_3O_{ads} + H_{ads} \tag{R26}$$

TiO_2^* here denotes an active site on the photocatalyst's surface. An important behavior needs to be pointed out here. As can be seen from R26, the adsorption of methanol on the TiO_2 surface is dissociative, making it strongly bonded to the surface [41]. However, for formaldehyde (R27), it is usually adsorbed via H-interaction, making its stability on the surface weaker. Once adsorbed, VOCs can undergo several degradation mechanisms:

$$CH_2O + TiO_2^* \rightarrow\ CH_2O_{ads} \tag{R27}$$

- For methanol [42].

$$CH_3O_{ads} + h^+ \rightarrow CH_2O_{ads} + H^+ \quad \text{(R28)}$$

$$CH_3O_{ads} + OH_{ads} \rightarrow CH_2O_{ads} + H_2O \quad \text{(R29)}$$

$$CH_3OH_{ads} + OH_{ads} \rightarrow CH_2OH_{ads} + H_2O \quad \text{(R30)}$$

$$CH_2OH_{ads} \rightarrow CH_2O_{ads} + H_{abs} \quad \text{(R31)}$$

- For formaldehyde [43].

$$CH_2O_{ads} + OH_{ads} \rightarrow HCO_{ads} + H_2O_{ads} \quad \text{(R32)}$$

$$CH_2O_{ads} + h^+ \rightarrow HCO_{ads} + H^+ \quad \text{(R33)}$$

$$HCO_{ads} + O_2^- \rightarrow HCOO_{ads}^- + O_{ads} \quad \text{(R34)}$$

$$HCOO_{ads}^- + h^+ \rightarrow CO_2 + H^+ \quad \text{(R35)}$$

Several pathways for the degradation of CH_3OH and CH_2O exist. But similarly to the discharge operating alone, one main outcome is observed for each species:

- For methanol, all the pathways lead to the formation of formaldehyde.
- For formaldehyde, all the pathways lead to the formation of $HCOO^-$ on the surface, which can be completely mineralized to CO_2 (R35).

The photocatalyst can also induce other reactions which can benefit the removal efficiency of the system [44]:

$$O_3 + e^-_{surf} \rightarrow O^- + O_2 \quad \text{(R36)}$$

$$O^- + H_2O \rightarrow OH + OH^- \quad \text{(R37)}$$

$$O_{2,\,ads} + e^-_{surf} \rightarrow O^-_{2,ads} \quad \text{(R38)}$$

$$O^-_{2,ads} + H^+ \rightarrow HO_{2,\,ads} \quad \text{(R39)}$$

R36 and R37 concern the photocatalytic degradation of ozone. The process again generates OH radicals which can be reused in the VOC degradation. Reaction R37 allows the creation of superoxide radicals on the TiO_2 surface, which can produce HO_2 (R39). This HO_2 is then desorbed and can feed the loop of reactions R13 – R17, oxidizing methanol, or generating OH radicals and hydrogen peroxide.

To sum up this part, the addition of the photoactivated TiO_2 brings new pathways for VOC degradation and generation of indirect oxidative species. Linking those mechanisms with the experimental section, especially Fig. 6b, brings some light on the higher removal efficiency obtained for methanol (40%) compared to formaldehyde (25%). Methanol is a well-known scavenger of holes in TiO_2 photocatalysis [45]. After being adsorbed on the surface of the TiO_2 (R26), methanol rapidly reacts with the holes on the surface, generating methoxy (CH_3O) and hydroxymethyl (CH_2OH) radicals. Those can further again react with holes on the surface (R28). This hole's consumption reduces the electron-hole recombination, prolonging the lifetime of surface electrons, which can promote the formation of other oxygen species on the surface (R25, R36, R38), and hence further oxidation pathways. Additionally, methanol has better adsorption on TiO_2 with direct dissociation, compared to formaldehyde which is weakly bonded to the surface (see R26 and R27). Finally, similarly to the gas phase reactions, all the degradation pathways of methanol lead to the formation of formaldehyde (R28 - R31). These three aspects together can explain the better removal of methanol compared to formaldehyde when the TiO_2 photocatalyst is added.

UV-induced NO_2 Formation

The last point of the reaction mechanism to address is the rise of NO_2 concentration occurring when the discharge is switched off and the UV-C lamps remain ignited, in the presence of TiO_2 (observed in Fig. 3b). At the same time, the removal efficiency of CH_3OH and CH_2O, before recovering after few minutes, coinciding with the NO_2 decay. To better understand this phenomenon, another experiment was performed to follow the NO_2 concentration

during the transition (DBD switched off). To separate the effects of DBD and UV-C lamps, the discharge was operating alone for 10 min (150 W), with 300 L.min^{-1} of air with the pollutants present. After 10 min, two conditions were tested. In the first case, the DBD was turned off, and 4 UV-C lamps ignited at the same time. In the second case, the DBD was turned off, and a delay of 10 min was introduced before igniting the 4 UV-C lamps. Note that, in the second case, the flow of air and pollutants was still running during the 10 min delay. Results for the first and second case are respectively shown in Fig. 7a and b.

The behavior of the NO_2 concentration is very similar in both cases. In Fig. 7a, when the DBD is turned off and the 4 UV-C lamps ignited simultaneously, the NO_2 rises directly. The concentration was measured just before the transition and no NO_2 was detected. The first point at 0 min corresponds to the first measurement and NO_2 starts to appear (it corresponds to a scanning time of 20 s, between t = 0 s and t = 20 s). The concentration is maximum at 1 min, with around 2 ppm of NO_2 detected. Then it decays and reaches around 0.5 ppm after 18 min. Due to the overlap with the growing water vapor bands in the infrared spectra, the estimation of the concentration at lower concentrations becomes unprecise. At this stage, it is not clear if the mechanisms involved are occurring in the gas phase or on the TiO_2 surface.

By inserting the 10 min delay between turning off the discharge and the 4 UV-C lamps ignition, the short-lived species from the gas phase are evacuated from the chamber, and hence only potentially surface-stored stable species remain. As can be observed on Fig. 7b, during the 10 min delay, no NO_2 is detected, as could be expected. At t = 10 min, the 4 UV-C are ignited, and the NO_2 concentration rises. In that case, the maximum concentration takes longer to reach than when the 4 UV-C lamps are ignited directly after DBD, around 3 min. This could be explained by the fact that some gas/surface mechanisms are occurring at the transition in the first case, while such mechanisms would be suppressed in the second case. But from the observation in Fig. 7b, the mechanisms are most likely related to species stored on the TiO_2 surface.

During the discharge phase, operating for 10 min before the 4 UV-C are ignited, NO_x are formed in the gas phase [46]:

$$O_2 + N \rightarrow NO + O \quad \text{(R40)}$$

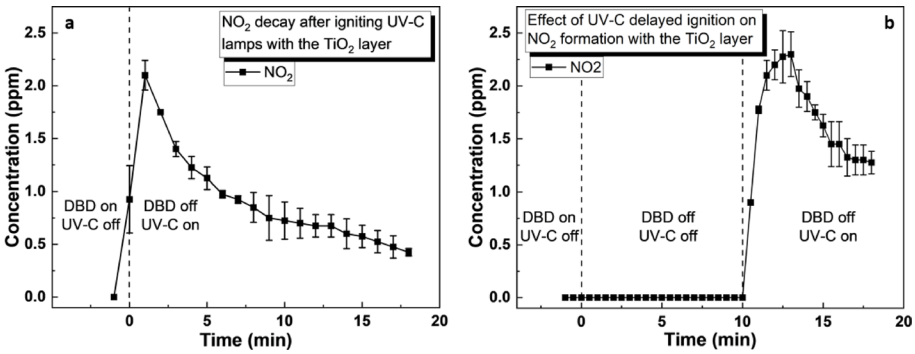

Fig. 7 Evolution of the NO_2 concentration after turning off the DBD, in presence of TiO_2, and igniting 4 UV-C lamps (a) immediately and (b) with 10 min delay

$$N_2 + O \rightarrow NO + N \quad \text{(R41)}$$

$$NO + O \rightarrow NO_2 \quad \text{(R42)}$$

$$NO_2 + O_3 \rightarrow NO_3 + O_2 \quad \text{(R43)}$$

$$NO_2 + O + M \rightarrow NO_3 + M \quad \text{(R44)}$$

$$NO_2 + NO_3 \rightarrow N_2O_5 \quad \text{(R45)}$$

NO_x species can interact and be adsorbed on the TiO_2 surface, even without UV-C activation [47–49]:

$$NO_{2,g} \rightarrow NO^-_{3,ads} \quad \text{(R46)}$$

$$NO_{3,g} \rightarrow NO^-_{3,ads} \quad \text{(R47)}$$

$$N_2O_{5,g} \rightarrow NO^-_{3,ads} \quad \text{(R48)}$$

The subscript "g" here denotes gas phase species. The exact adsorption reactions (R46 – R48) will not be described here, but they involve reactions such as adsorbed hydroxyl or water molecules, collisions with the surface and charge compensation, or hydrolysis. The main outcome is that all the NO_x generated species from the discharge can lead to the formation of surface nitrates, even in the absence of UV activation of the TiO_2. When illuminating the TiO_2 with UV-C, the electron hole pairs are generated (R23), and the holes can neutralize the charge from the nitrates, producing a radical, which can then desorb to NO_2 [50]:

$$NO^-_{3,ads} + h^+ \rightarrow NO_{3,ads} \quad \text{(R49)}$$

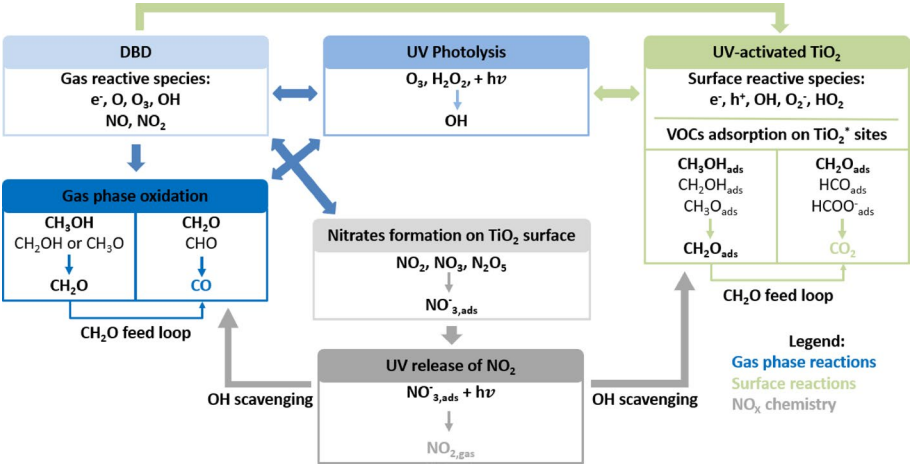

Fig. 8 Schematic of the main reactive species and interactions between the different components of the system

$$NO_{3,ads} + hv \rightarrow NO_{2,g} + O_{ads} \quad \text{(R50)}$$

Once the electron from the nitrate is removed by the hole (R49), a nitrate radical is formed, which is decomposed under UV illumination, desorbing nitrogen dioxide in the gas phase (R50). This explains the NO_2 increase after switching on the 4 UV-C lamps in Fig. 7a and b. The influence of the number of UV-C lamps ignited, i.e., 2 or 4 UV-C lamps, on the NO_2 release was also tested (results not shown). While the behavior was the same and the NO_2 peak appeared after the lamp ignition, the concentration rise was steeper and reached higher values when 4 UV-C lamps were activated. Such an effect is more likely due to the higher UV radiation, which is expected from R50. The rise of the catalyst temperature could also play a role here; however, it might still be negligible compared to the effect of the doubled UV radiation (2 vs. 4 lamps).

The NO_2 peak observed was also seen to coincide with a decrease of CH_3OH and CH_2O in Fig. 4a and b. This phenomenon can be explained by the scavenging of OH radicals by NO_2 [51]:

$$NO_2 + OH \rightarrow HNO_3 \quad \text{(R51)}$$

As NO_2 reacts with OH radicals just after their production by the 4 UV-C lamps ignition following reaction R51, the removal efficiency of both VOCs is partially lowered, and it finally recovers slowly as the nitrates on the surface of the TiO_2 are consumed.

The main reactive species, generated by the different components of the system, as well as the interactions between them, have been summarized and are shown in Fig. 8.

Conclusion

This work presents the recent experimental advances carried out on an indoor air decontamination system combining a dielectric barrier discharge with UV-C activated titanium dioxide, used for treating large air flows up to 300 $L.min^{-1}$. In the first part, the performance of the system during the simultaneous removal of methanol and formaldehyde was assessed. It was shown that, while testing the different components separately, the synergy between the discharge and the UV-C lamps was beneficial to the removal, especially for CH_2O, even when no TiO_2 was present.

The FTIR analysis of the gas effluent revealed several species generated by the discharge (N_2O, NO_2, O_3, N_2O_5), as well as CO originating from the mineralization of the pollutants. As the system used the ambient air with its much higher background concentration, CO_2 could not be measured but is also a likely byproduct of VOC degradation. Two relative humidities (30% vs. 60%) were tested. While the trends were similar in both cases, the higher relative humidity led to an improved removal efficiency due to the higher generation of hydroxyl radicals. The role of TiO_2 was also investigated in this configuration. When the discharge was combined with 4 UV-C lamps, without TiO_2, CH_2O was preferentially removed (50% efficiency against 30% for CH_3OH). Inversely, when TiO_2 was present, it benefited more towards methanol removal, although both pollutants reached similar efficiency (40%). The partial carbon balance indicated that the main byproduct was CO, but the activated photocatalyst seemed to slightly enhance the complete mineralization towards CO_2.

Finally, the effect of the specific input energy was tested. For the discharge operating alone, both with and without TiO_2, the removal efficiency was similar and increased with the rising SIE. However, when combining with the UV-C, results showed different selectivity on both VOCs depending on the presence or absence of TiO_2. Especially with photocatalyst, methanol removal improved significantly when increasing SIE, while this increase was less remarkable for both pollutants when the TiO_2 was not present.

The second part of the work detailed the reaction mechanisms occurring in the system, linked with the various components operation. Globally, it was shown that the methanol conversion pathways all lead to the formation of formaldehyde. This hence limits the actual conversion of the formaldehyde that was initially injected into the air steam. Additionally to the direct oxidation of the pollutants by oxygen atoms and hydroxyl radicals, several sources and potential reservoirs of hydroxyl radicals were identified that can be involved in the removal efficiency boosting, when UV and TiO_2 were present. The most important ones seem to be reactions involving HO_2, as well as H_2O_2 and O_3 photolysis. Finally, an interesting phenomenon was observed when the discharge operated for some time and was then turned off, and the UV-C lamps were subsequently ignited. At this transition, the NO_2 concentration rapidly increased, and then slowly decayed. This effect was explained by the conversion of NO_x (NO_2, NO_3, N_2O_5) formed in the gas phase to surface nitrates (NO_3^-) on the TiO_2, even without UV activation. These nitrates were then reconverted to NO_2 and desorbed when the UV-C lamps were ignited, partially scavenging OH radicals and reducing the removal efficiency of pollutants.

This work showed promising results in terms of removal efficiency against low concentrations of indoor air pollutants, especially considering the large flow rates and operation in ambient air. By identifying the main reactions involved depending on the operating com-

ponents of the system, further development can help tune the performance of the indoor air plasma-photocatalytic cleaning system to target specific pollutants. Improvement needs to be made to reduce undesirable byproducts such as CO, O_3 or NO_2, and to further improve the removal efficiency and energy yield of the system.

Acknowledgements This work was funded by the EU NextGenerationEU through the Recovery and Resilience Plan for Slovakia under the project 09I03-03-V03-00033 EnvAdwice, and Slovak Research and Development Agency grant APVV-22-0247.

Author contributions A.D. carried out the experiments and analyses, processed and interpreted the data, and wrote the original and revised manuscript. Z.M. conceptualized and supervised the research, secured funding, contributed to the result analyses and interpretations, and revised the manuscript. Both authors reviewed the manuscript.

Funding Open access funding provided by The Ministry of Education, Science, Research and Sport of the Slovak Republic in cooperation with Centre for Scientific and Technical Information of the Slovak Republic

Data Availability No datasets were generated or analysed during the current study.

Declarations

Competing interests The authors declare no competing interests.

References

1. World Health Organization. Household Air Pollution. https://WwwWhoInt/News-Room/Fact-Sheets/Detail/Household-Air-Pollution-and-Health 2025.
2. United States Environmental Protection Agency. Volatile Organic Compounds' Impact on Indoor Air Quality. https://WwwEpaGov/Indoor-Air-Quality-Iaq/Volatile-Organic-Compounds-Impact-Indoor-Air-Quality 2025.
3. Obitková D, Mráz M, Pavlík E (2024) Virus removal by high-efficiency air (HEPA) filters and filtration capacity enhancement by nanotextiles: a pilot study. Folia Microbiol (Praha) 69:459–464. https://doi.org/10.1007/s12223-024-01137-4
4. Yu L, Duan Y, Wang D, Liang Z, Liang C, Wang Y (2025) Recent advances in TiO2 modification for improvement in photocatalytic purification of indoor VOCs. RSC Adv 15:28204–28230. https://doi.org/10.1039/d5ra02935j
5. Wei Y, Wu Q, Meng H, Zhang Y, Cao C (2023) Recent advances in photocatalytic self-cleaning performances of TiO2-based building materials. RSC Adv 13:20584–20597. https://doi.org/10.1039/d2ra07839b
6. Hanif MA, Shin H, Chun D, Kim HG, Kwac LK, Kim YS (2023) Photocatalytic VOCs Degradation Efficiency of Polypropylene Membranes by Incorporation of TiO2 Nanoparticles. Membr (Basel) 13. https://doi.org/10.3390/membranes13010050
7. Wang W, Zhang D, Sun P, Ji Z, Duan J High efficiency photocatalytic degradation of indoor formaldehyde by Ag/g-C3N4/TiO2 composite catalyst with ZSM-5 as the carrier. Microporous Mesoporous Mater 2021;322. https://doi.org/10.1016/j.micromeso.2021.111134

8. Song J, Ren X, Hu G, Wang L, Hu X Enhanced photocatalytic degradation of indoor formaldehyde by sepiolite decorated with TiO2 nanoparticles: Effects of key preparation parameters. Microporous Mesoporous Mater 2023;353. https://doi.org/10.1016/j.micromeso.2023.112515
9. Urashima K, Chang J-S (2000) Sources Effects Removal of Volatile Organic Compounds from Air Streams and Industrial Flue Gases. IEEE Trans Dielectr Electr Insul ;7
10. Kim HH (2004) Nonthermal plasma processing for air-pollution control: A historical review, current issues, and future prospects. Plasma Processes Polym 1:91–110. https://doi.org/10.1002/ppap.200400028
11. Asilevi PJ, Boakye P, Oduro-Kwarteng S, Fei-Baffoe B, Sokama-Neuyam YA Indoor air quality improvement and purification by atmospheric pressure Non-Thermal Plasma (NTP). Sci Rep 2021;11. https://doi.org/10.1038/s41598-021-02276-1
12. Mustafa MF, Fu X, Liu Y, Abbas Y, Wang H, Lu W (2018) Volatile organic compounds (VOCs) removal in non-thermal plasma double dielectric barrier discharge reactor. J Hazard Mater 347:317–324. https://doi.org/10.1016/j.jhazmat.2018.01.021
13. Saleem F, Rehman A, Ahmad F, Khoja AH, Javed F, Zhang K et al (2021) Removal of toluene as a toxic VOC from methane gas using a non-thermal plasma dielectric barrier discharge reactor. RSC Adv 11:27583–27588. https://doi.org/10.1039/d1ra04772h
14. Dahiru UH, Saleem F, Zhang K, Harvey A (2022) Plasma-assisted removal of methanol in N2, dry and humidified air using a dielectric barrier discharge (DBD) reactor. RSC Adv 12:10997–11007. https://doi.org/10.1039/d2ra01097f
15. Belkessa N, Assadi AA, Bouzaza A, Nguyen-Tri P, Amrane A, Khezami L (2024) A review of non-thermal plasma -catalysis: The mutual influence and sources of synergetic effect for boosting volatile organic compounds removal. Environ Res 257. https://doi.org/10.1016/j.envres.2024.119333
16. Bogaerts A, Tu X, Whitehead JC, Centi G, Lefferts L, Guaitella O et al The 2020 plasma catalysis roadmap. J Phys D Appl Phys 2020;53. https://doi.org/10.1088/1361-6463/ab9048
17. Li M, Li D, Zhang Z, Ji C, Zhou S, Guo W et al (2021) Study on the performance and mechanism of degradation of toluene with non-thermal plasmas synergized supported TiO2/γ-Al2O3catalyst. J Environ Chem Eng 9. https://doi.org/10.1016/j.jece.2021.105529
18. Jangra R, Ahlawat K, Prakash R (2023) An SDBD plasma-based source for efficient degradation of VOCs in an enclosed environment. Phys Lett Sect A: Gen At Solid State Phys 490. https://doi.org/10.1016/j.physleta.2023.129184
19. Vazquez T, Lavrikova A, Wiedermann D, Babic J, Palko M, Palko M et al (2025) Non-thermal plasma coupled with photocatalysis for indoor air treatment at high air flow rates: effects on VOCs and bioaerosols. J Electrostat 138. https://doi.org/10.1016/j.elstat.2025.104160
20. Floran Peeters and Tom Butterworth Electrical Diagnostics of Dielectric Barrier Discharges. Atmospheric pressure plasma - From diagnostics to applications, 2019 (Book, IntechOpen). https://doi.org/10.5772/intechopen.80433
21. He Y, Shen J, Alharbi NS, Chen C (2023) Volatile organic compounds degradation by nonthermal plasma: a review. Environ Sci Pollut Res 30:32123–32152. https://doi.org/10.1007/s11356-023-25524-5
22. Remy A, De Geyter N, Reniers F Interplay between nitrogen oxides and ozone in a filamentary dielectric barrier discharge at various frequencies. Plasma Processes Polym 2023;20. https://doi.org/10.1002/ppap.202200201
23. Ma T, Zhao Q, Liu J, Zhong F (2016) Study of humidity effect on benzene decomposition by the dielectric barrier discharge nonthermal plasma reactor. Plasma Sci Technol 18:686–692. https://doi.org/10.1088/1009-0630/18/6/17
24. Asilevi PJ, Yi CW, Li J, Nawaz MI, Wang HJ, Yin L et al (2020) Decomposition of formaldehyde in strong ionization non-thermal plasma at atmospheric pressure. Int J Environ Sci Technol 17:765–776. https://doi.org/10.1007/s13762-019-02476-3
25. Dhakal OB, Dahal R, Lamichhane P, Acharya TR, Choi EH (2024) Gas phase formaldehyde degradation: Continuous versus duty cycle driven plasma reactor. Process Saf Environ Prot 190:744–754. https://doi.org/10.1016/j.psep.2024.07.089
26. Norsic C, Tatibouët JM, Batiot-Dupeyrat C, Fourré E (2018) Methanol oxidation in dry and humid air by dielectric barrier discharge plasma combined with MnO2-CuO based catalysts. Chem Eng J 347:944–952. https://doi.org/10.1016/j.cej.2018.04.065
27. Yao S, Zhang X, Lu B (2005) Influence of plasma reactor structure on methanol oxidation. AIChE J 51:1558–1564. https://doi.org/10.1002/aic.10450
28. Lee DH, Kim T (2014) Effect of catalyst deactivation on kinetics of plasma-catalysis for methanol decomposition. Plasma Processes Polym 11:455–463. https://doi.org/10.1002/ppap.201300185
29. Ding HX, Zhu AM, Yang XF, Li CH, Xu Y (2005) Removal of formaldehyde from gas streams via packed-bed dielectric barrier discharge plasmas. J Phys D Appl Phys 38:4160–4167. https://doi.org/10.1088/0022-3727/38/23/004

30. Storch DG, Kushner MJ (1993) Destruction mechanisms for formaldehyde in atmospheric pressure low temperature plasmas. J Appl Phys 73:51–55. https://doi.org/10.1063/1.353828
31. IUPAC. Task Group on Atmospheric Chemical Kinetic Data Evaluation - Data Sheet I.A3.45 NOx15. n.d
32. IUPAC (2001) Task Group on Atmospheric Chemical Kinetic Data Evaluation - Data Sheet HOx14
33. IUPAC Task Group on Atmospheric Chemical Kinetic Data Evaluation – Data Sheet HOx5. n.d
34. Zhang X, Lee BJ, Im HG, Cha MS (2016) Ozone Production with Dielectric Barrier Discharge: Effects of Power Source and Humidity. IEEE Trans Plasma Sci 44:2288–2296. https://doi.org/10.1109/TPS.2016.2601246
35. Matsumi Y, Kawasaki M (2003) Photolysis of Atmospheric Ozone in the Ultraviolet Region. Chem Rev 103:4767–4781. https://doi.org/10.1021/cr0205255
36. Dunlea EJ, Ravishankara AR (2004) Measurement of the rate coefficient for the reaction of O(1D) with H2O and re-evaluation of the atmospheric OH production rate. Phys Chem Chem Phys 6:3333–3340. https://doi.org/10.1039/b402483d
37. Vione D, Maurino V, Minero C, Pelizzetti E (2003) The atmospheric chemistry of hydrogen peroxide: a review. Ann Chim ;93
38. Li YW, Ma WL Photocatalytic oxidation technology for indoor air pollutants elimination: A review. Chemosphere 2021;280. https://doi.org/10.1016/j.chemosphere.2021.130667
39. Setvin M, Hulva J, Wang H, Simschitz T, Schmid M, Parkinson GS et al (2017) Formaldehyde Adsorption on the Anatase TiO2(101) Surface: Experimental and Theoretical Investigation. J Phys Chem C 121:8914–8922. https://doi.org/10.1021/acs.jpcc.7b01434
40. Setvin M, Shi X, Hulva J, Simschitz T, Parkinson GS, Schmid M et al (2017) Methanol on anatase TiO2 (101): Mechanistic insights into photocatalysis. ACS Catal 7:7081–7091. https://doi.org/10.1021/acscatal.7b02003
41. Yuan Q, Wu Z, Jin Y, Xu L, Xiong F, Ma Y et al (2013) Photocatalytic cross-coupling of methanol and formaldehyde on a rutile TiO2(110) surface. J Am Chem Soc 135:5212–5219. https://doi.org/10.1021/ja400978r
42. Panayotov DA, Burrows SP, Morris JR (2012) Photooxidation mechanism of methanol on rutile TiO 2 nanoparticles. J Phys Chem C 116:6623–6635. https://doi.org/10.1021/jp209215c
43. Tasbihi M, Bendyna JK, Notten PHL, Hintzen HT (2015) A short review on photocatalytic degradation of formaldehyde. J Nanosci Nanotechnol 15:6386–6396. https://doi.org/10.1166/jnn.2015.10872
44. Destrieux A, Jangra R, Hensel K, Machala Z (2025) Review on scientific studies and commercial indoor air purification devices: Focus on plasma-catalytic technology. J Electrostat. https://doi.org/10.1016/j.elstat.2025.104153
45. Henderson MA (2011) A surface science perspective on TiO2 photocatalysis. Surf Sci Rep 66:185–297. https://doi.org/10.1016/j.surfrep.2011.01.001
46. Shaban M, Merkert N, van Duin ACT, van Duin D, Weber AP (2024) Advancing DBD Plasma Chemistry: Insights into Reactive Nitrogen Species such as NO2, N2O5, and N2O Optimization and Species Reactivity through Experiments and MD Simulations. Environ Sci Technol 58:16087–16099. https://doi.org/10.1021/acs.est.4c04894
47. Sivachandiran L, Thevenet F, Rousseau A, Bianchi D (2016) NO2 adsorption mechanism on TiO2: An in-situ transmission infrared spectroscopy study. Appl Catal B 198:411–419. https://doi.org/10.1016/j.apcatb.2016.05.065
48. Bertram TH, Thornton JA (2009) Toward a general parameterization of N 2 O 5 reactivity on aqueous particles: the competing effects of particle liquid water, nitrate and chloride. Atmos Chem Phys 9:8351–8363. https://doi.org/10.5194/acp-9-8351-2009
49. Mahmood A, Wang X, Xie X, Sun J (2021) Adsorption of NO2 and subsequent formation of nitrate species in the dark on TiO2 nanoparticles exhibiting different morphologies: An in-situ FTIR study. Colloids Surf Physicochem Eng Asp 626. https://doi.org/10.1016/j.colsurfa.2021.127058
50. Bedjanian Y, El Zein A (2012) Interaction of 2 with TiO 2 surface under UV irradiation: Products study. J Phys Chem A 116:1758–1764. https://doi.org/10.1021/jp210078b
51. Tsang W, Herron JT, Reactions Involving NO NO2, HNO, HNO2, HCN and N2O. J Phys Chem Ref Data 1991;20. https://doi.org/10.1063/1.555890